Investigation of recombination mechanisms of CdTe solar cells with different buffer layers

Xiaohui Fang, Shengqiang Ren, Chunxiu Li, Chuang Li, Gang Chen, Huagui Lai, Jingquan Zhang, Lili Wu*

College of Materials Science and Engineering, Sichuan University, Chengdu 610065, China

ARTICLE INFO

ABSTRACT

It is critical to understand the dominant recombination mechanisms of thin film solar cells for further improving their performance. The dominant recombination paths of CdTe solar cells with Mg$_x$Zn$_{1-x}$O (MZO), MZO/CdS and MZO/CdS/CdSe buffer layers were investigated by temperature-dependent current-voltage (JVT) characterization both in light and dark, with traditional CdS/CdTe devices as a reference. The devices with MZO or MZO/CdS buffer layers are confirmed to be dominated by interface recombination, which leads to poor performance of devices. Compared to devices with traditional CdS buffer layers which are dominated by bulk recombination, the devices with MZO/CdS/CdSe buffer layer exhibit the same dominant recombination path but superior performance. It demonstrates that MZO/CdS/CdSe can be a promising composite buffer layer.

1. Introduction

Cadmium telluride (CdTe) thin film solar cells have seen a rapid development in recent years with a record efficiency up to 22.1% [1]. To improve the efficiency of CdTe solar cells, many efforts have been made in finding alternative buffer layers to replace conventional CdS layer. One promising material for this application is Mg$_x$Zn$_{1-x}$O (MZO). MZO was first used as a buffer layer for CIGS solar cells in 2003 [2], later in CdTe [3]. The bandgap of MZO can be adjusted from 3.3 eV to 6.7 eV with increasing magnesium content. The introduction of MZO layer can eliminate blue loss induced by CdS optical absorption and lead to a higher V_{oc} [4]. More importantly, MZO has a lower electronic affinity which is desirable for forming the front contact and minimizing the interface recombination at the front CdTe interface [5]. However, due to the weak diode and insufficient built-in potential between MZO and CdTe, an ultrathin CdS film may be necessary [6]. Another important buffer layer material is CdSe which can enhance the photocurrent in both short and long wavelength regions of CdTe solar cells. A combined CdS/CdSe buffer layer can realize high V_{oc} while maintaining the increase of photo-current [7]. In this work, MZO, MZO/CdS and MZO/CdS/CdSe are applied as buffer layers of CdTe solar cells.

To understand the role of different buffer layers and carrier transport mechanisms, it is expected to shed light on the dominant recombination paths in the cells. By performing current-voltage (J-V) measurements over temperature or light intensity, one can identify and distinguish different recombination paths through the functional dependence. This approach has long been used in CIGS [8,9], CZTSSe [10], CdTe [11] and other solar cells [12,13]. Major et al. [11] found that the chloride treatments can reduce the CdS/CdTe interface recombination and improve the short current density and fill factor. Recently, most of the works focus on investigating the recombination in CdS/CdTe solar cells, few about MZO-buffer/CdTe solar cells. In this work, temperature-dependent current-voltage (JVT) measurements are used to identify and separate out the recombination mechanisms in CdTe solar cells with different buffer layers, over the temperature range of 300–355 K both in light and dark. Meanwhile, time-resolved photoluminescence (TRPL) is utilized to verify the recombination process. The devices with MZO, MZO/CdS, MZO/CdS/CdSe buffer layers are measured with traditional CdS buffer layer as a reference. The analysis helps us better understand the performance of cells and provides further theoretical guidance for the fabrication of high efficiency CdTe solar cells.

2. Theory

The basic diode behavior and recombination mechanisms of all the thin-film solar cells are same [14]. Current-voltage measurement is the most common tool for characterizing the performance of solar cells, and it is fast, easily accessible and accurate. Except for the determination of basic parameters, it contains a wealth of additional information,

especially when the dependence of temperature and light intensity is considered.

The current-voltage behavior of thin film solar cells can be generally described by the one-diode model

$$J = J_0 \left[exp\left(\frac{q(V - R_s J)}{AkT} \right) - 1 \right] + G(V - R_s J) - J_L, \tag{1}$$

where A is the diode ideality factor, k is the Boltzmann constant, T is the temperature, R_s and G are series resistance and shunt conductance, respectively. J_L is the light-induced current density which is constant in this case.

The diode current J_0 can be given by

$$J_0 = J_{00} \exp\left[\frac{-E_a}{AkT} \right], \tag{2}$$

where E_a is an activation energy associated with recombination in solar cells, J_{00} is the reference current density which is temperature-independent. Depending on the recombination pathways, different values for A, J_{00} and E_a can be obtained.

Combining Eqs. (1) and (2), at open circuit conditions where J is zero, the open-circuit voltage can be written as

$$V_{oc} = \frac{E_a}{q} + \frac{AkT}{q} \ln\left(\frac{J_L}{J_{00}} - \frac{V_{oc} G}{J_{00}} \right). \tag{3}$$

A shunt conductance G of 10^{-3} S cm^{-2} is 100 times smaller than the quotient J_L / V_{oc}, therefore, by setting G to zero, the ideal expression of the open-circuit voltage is

$$V_{oc} = \frac{E_a}{q} - \frac{AkT}{q} \ln\left(\frac{J_{00}}{J_L} \right). \tag{4}$$

The activation energy is important to distinguish the dominant recombination path between interface and bulk. Fig. 1 displays the main three recombination mechanisms that can occur in CdTe solar cells. For a heterojunction of high quality, the activation energy is provided by the bandgap of the absorber, that is, the recombination in the space charge region and neutral region, which is the bulk mechanisms 2 and 3 shown in Fig. 1. However, lower activation energy can also result in recombination at the interface due to conduction band miss alignment or Fermi level pinning [15], that is, interface recombination mechanism 1 illustrated in Fig. 1.

Several methods have been used to deduce the activation energy [16]. It is a common way to extract the activation energy by extrapolating V_{oc} to 0 K and no one-diode model parameters are required, so less fitting errors are introduced. It must be noted that only if the diode quality factor is temperature independent and the photo current collection is not reduced too much at V_{oc}, the determination of activation energy can be effective. Obviously, this method is not applicable in dark. According to Eq. (2), the quantity $A\ln(J_0)$ is plotted as a function
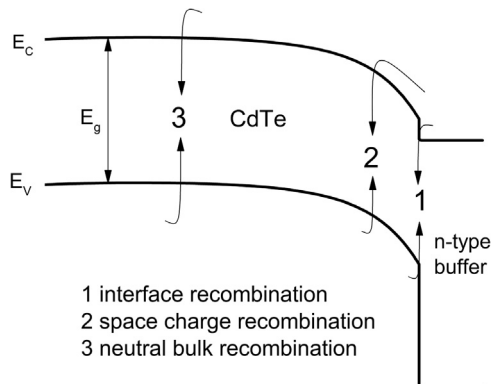

Fig. 1. Schematic band diagram of CdTe solar cell showing the three main recombination mechanisms that can occur.

of the inverse thermal energy $1/kT$, so the activation energy can be extracted as the slop of a linear fit to these data. In this work, we applied these two methods to calculate the activation energy in light and dark, respectively.

3. Experimental details

3.1. Device fabrication

The structure of the measured devices is glass/FTO/buffer/CdTe/ZnTe:Cu/Au. Except for buffer layers, the preparation processes were all the same for measured devices. The substrates (Pilkington Tec10) were cleaned with Amway glass cleaner, rinsed in deionized water and then with ultrasonic cleaning. CdS thin films were prepared by chemical bath deposition (CBD) as reported [17]. $Mg_xZn_{1-x}O$ layers (80 nm) were deposited by radio frequency magnetron sputtering with a ceramic target (mixed with ZnO and MgO powder) at a composition of $x \sim 0.18$. CdSe thin films (80 nm) were deposited by magnetron sputtering with 100 W RF power at 550 °C substrate temperature and in an argon ambient of 10 mTorr. CdTe thin films were deposited by close-space sublimation (CSS) at a source temperature of 630 °C with a thickness of ~ 4 μm. After the CdTe deposition, the surface of CdTe films was treated by CdCl$_2$ solution and then annealed at 388 °C for 35 min in N$_2$/O$_2$ atmosphere to enhance the lifetime of charge carriers and passivate grain boundaries [18]. After the CdCl$_2$ treatment, all devices were etched in 0.2% Br/CH$_3$OH solution for 8 s to remove surface oxides and to create a Te-rich surface. Then ZnTe:Cu films were deposited by vacuum co-evaporation with a thickness of 70 nm, with $\sim$ 6% copper concentration. Rapid thermal process of ZnTe:Cu was performed in nitrogen atmosphere from room temperature to ~ 360 °C in 90 s. Devices were completed by evaporating ~ 100 nm of Au as a back electrode. The area of measured devices was determined by a laser scriber with 0.24 cm^2.

3.2. Characterization

The temperature-dependent J-V characteristics of CdTe solar cells with different buffer layers were performed both in light and dark. The light JVT was performed using a pulsed light solar simulator under AM1.5 with a Xe lamp, which was calibrated with a GaAs standard cell. The light-induced temperature gradient across the samples can be negligible. The Agilent 4155 C semiconductor parameter analyzer was used in dark JVT measurement. The temperature was varied from 300 K to 355 K with increments of 5 K. The device was heated by a home-made resistive heater and the temperature of device was controlled individually by an adhesive thermocouple (ST-50, PKC, Inc.) which is stuck on the substrate as close as possible to the measured cell, with 0.1 K accuracy or better. The external quantum efficiency (EQE) was performed by QEX10 (PV Measurement, Inc.) in the wavelength range of 280–1000 nm. Time-resolved photoluminescence (TRPL) was performed by FLS980 (Edinburgh Instrument, Inc.) at room temperature. Excitation at 633 nm with 98 ps pulses as well as 4 MHz laser repetition were used.

4. Results and discussion

Due to the high Schottky barrier in the devices, solar cells without back contacts cannot fit into the one-diode model, which results in a failure in JVT measurements. Therefore, all the samples with back contacts are analyzed in this work. For some devices, at low temperatures (below 250 K), the free carriers freeze-out and the quasi-Fermi levels no longer respond to changes in temperature [19]. It is evident that the open-circuit voltage converges to a plateau and no longer increases below 250 K [20]. At high temperatures, solar cells show a proper one diode. Hence, the temperature from 300 K to 355 K was applied to obtain a better linear relationship. For devices with different

Table 1
J-V parameters of the devices measured in AM1.5 at room temperature.

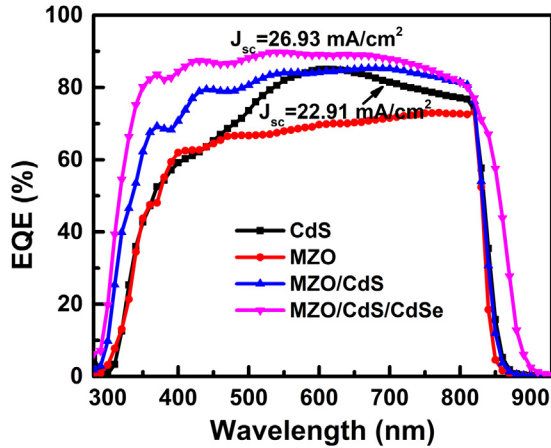| Sample	Eff (%)	R_{sh} ($\Omega\,cm^2$)	R_s ($\Omega\,cm^2$)	FF (%)	J_{sc} (mA/cm^2)	V_{oc} (mV)
CdS	14.13	2452.32	3.71	72.76	24.45	794.32
MZO	8.25	221.52	7.99	59.04	20.97	666.24
MZO/CdS	11.01	424.54	6.04	60.26	27.55	663.30
MZO/CdS/CdSe	15.37	832.88	4.24	69.79	27.72	794.88

Fig. 2. External quantum efficiency of CdTe solar cells with different buffer layers.

buffer layers, we have measured more than 5 samples with the same structure to confirm the repeatability.

The J-V parameters of devices are showed in Table 1 and the corresponding EQE curves are seen in Fig. 2. CdTe cells with MZO buffer layers are not expected as reported [21]. The spectral response of the MZO cell in CdTe region (550–800 nm) is significantly lower than other three devices, which clearly indicates that there is no high-quality p-n junction between MZO and CdTe. To enhance the built-in potential, an ultrathin CdS film (~ 30 nm) was introduced between the MZO and CdTe layer. Compared with traditional CdS cells, the structure of MZO/CdS greatly enhances the spectral response in short wavelength region (300–550 nm), but the V_{oc} of device is still low. However, the performance of CdTe solar cells is greatly improved after applying a MZO/CdS/CdSe composite buffer layer. The EQE curve exhibits a higher collection in short wavelength region and a superior blue response. Meanwhile, due to the formation of CdTe$_{1-x}$Se$_x$ in fabrication process of CdTe solar cells, the absorption edge shows a redshift. With enhanced spectral response in both short and long wavelength regions, the current collected by the device with MZO/CdS/CdSe buffer layer increases by 4.01 mA/cm^2 than that of the traditional CdS cells.

Fig. 3 shows current-voltage characteristics of CdTe solar cells at various temperatures in AM1.5. It presents that all devices behave well in the range of 300–355 K. The J_{sc} increases for the reduction of bandgap with increasing temperature, which facilitates more low-energy photons to be absorbed [22]. In all cases, the series and shunt resistances have almost no effect on cells. The temperature dependence of J-V curves of solar cells is derived from the temperature dependence of equilibrium concentrations of charge carriers. With the temperature increasing, the intrinsic carrier concentration increases exponentially as well as the dark current, thus reducing the open circuit voltage. The V_{oc} collected as a function of temperature in the range of 300–355 K is showed in Fig. 4. The V_{oc} versus temperature follows a straight line well for all devices and the extrapolation results of activation energy are lower than bandgap of CdTe to varying degrees.

The conduction band offset ΔE_c between the buffer layer and the absorber layer is given by
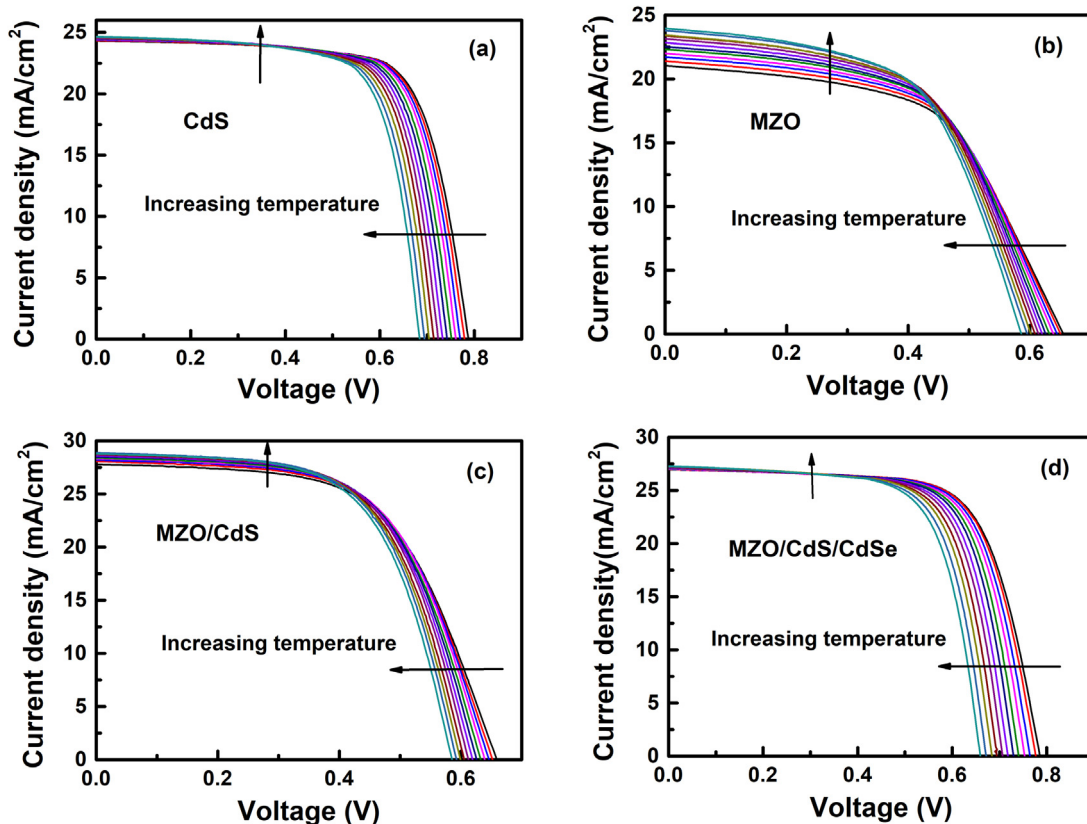

Fig. 3. Current-voltage characteristics of CdTe solar cells with different buffer layers at various temperatures in AM1.5.
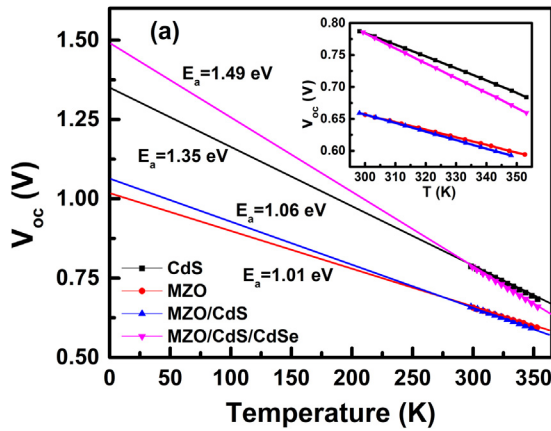
Fig. 4. Temperature dependent open circuit voltage (V_{oc}) and its linear extrapolation line to 0 K. The inset image is an enlarged view of V_{oc} *vs. T* between 300 and 355 K.

$$\Delta E_c = E_c^{buffer} - E_c^{absorber}, \tag{5}$$

where E_C^{buffer} ($E_C^{absorber}$) is the conduction band minimum of the buffer (absorber). Such that a positive value is often referred to as a "spike" and a negative value as a "cliff". The case of $E_a < E_g$ is usually considered to be related to the negative conduction band offset [8]. The ideal heterojunction front contact of CdTe solar cells is to maximize the built-in potential and minimize the interfacial recombination at the buffer/absorber interface. To accomplish this, a flat or a small and positive conduction band offset ($\Delta E_c > 0$, spike) is necessary; while a negative conduction band offset ($\Delta E_c < 0$, cliff) would reduce built-in potential and increase interface recombination. For $\Delta E_c < 0$, even a small interface recombination velocity V_{intf} can lead to large interface recombination and a limited V_{oc}. Hence, it is important to engineer ΔE_c to produce a spike in 0.1–0.4 eV range [23]. One of the considerations of using MZO as a buffer layer is that it can achieve favorable band alignment with CdTe. By varying thickness and composition of the MZO layer, both cliff and spike behavior could be demonstrated.

The bandgap of pure CdTe absorber is about 1.5 eV. The obtained value of E_a for the CdS/CdTe device is slightly lower than the bandgap, thus it is difficult to estimate that the dominant recombination path is interface or bulk recombination. The interface recombination limits V_{oc} significantly, especially occurs in CZTSe and CIGS solar cells with CdS buffer layers that exhibit many defect states [10]. The CdS/CdTe interface is in the cliff category [24], and the conduction band offset is approximately − 0.1 eV [25], which may lead to interface recombination. However, the value for E_a slightly below the bandgap of absorber is also observed in other studies [10], and Delahoy et al. [26] regards this as the formation of CdTe$_{1-x}$S$_x$ compound in CdTe solar cells. The fabrication process of CdS/CdTe solar cells leads to intermixing of CdS and CdTe layers, thus the formation of CdTe$_{1-x}$S$_x$ compound, and the bandgap of CdTe$_{1-x}$S$_x$ decreases below the CdTe bandgap to as low as 1.41 eV at x ~ 0.3, before increasing at higher x values [27]. Therefore, considering the existence of CdTe$_{1-x}$S$_x$ and the high V_{oc} as well as good performance of CdS/CdTe devices, the dominant recombination path can be inferred as bulk recombination.

The value of E_a for the device with MZO buffer layer is much smaller than bandgap, only about 1.01 eV, indicating that the dominant recombination path is interface recombination, which is consistent with the low V_{oc} and poor performance in Table 1. The interface recombination is not only affected by band alignment at the emitter/absorber interface, but also by emitter property and interface defects [24]. We have expected that the MZO (x ~ 0.18) film can achieve a positive conduction band offset with CdTe to suppress the interface recombination. However, the experimental results show that the fabricated MZO film has lots of surface states. The quality of MZO thin film

can be influenced by growth temperature and oxygen partial pressure during sputter deposition [28], and the property may change in subsequent fabrication of CdTe cells. The resistivity of the as-grown MZO films is so high that it exceeds the measurement range ($> 10^8 \, \Omega \, cm$), but after rapid thermal annealing process, the electrical properties of MZO films change a lot [29]. Thus, we infer that surface states of the MZO film are the main factor affecting the heterojunction interface, which leads to dominant interface recombination for MZO/CdTe devices.

The device with MZO/CdS buffer layer yields an activation energy of 1.06 eV, indicating that the dominant recombination path is still interface recombination, which significantly limits V_{oc} and FF of the device. On the one hand, the thickness of CdS is only 30 nm, and the open circuit voltage and fill factor may suffer from pinholes by reducing the CdS thickness, which has been reported by other studies [30,31]. For another, the MZO/CdS interface is much different from the MZO/CdTe interface. Rao at al. [32] demonstrated a flat conduction band alignment between CdS and Zn$_{0.85}$Mg$_{0.15}$O. Considering defects in CdS films, we assume that the recombination at MZO/CdS interface to be dominant. This could be possible in the case of a weak type inversion at CdTe surface [33]. Further investigation is needed to improve the understanding of this mechanism.

A noteworthy finding is that the activation energy increases after the introduction of CdSe. The value of E_a for the device with MZO/CdS/CdSe buffer layer is 1.49 eV, which is very close to the bandgap of CdTe. Compared to devices with MZO and MZO/CdS buffer layers, the dominant recombination path has changed from interface combination to bulk recombination and the V_{oc} of devices has been improved largely, closely to the CdS/CdTe devices (~ 800 mV). The CdS/CdTe interface is more dissolved to find any interface for CdS/CdTe solar cells, which leads to the bulk recombination. So does the CdS/CdSe/CdTe interfaces. Either the introduction of CdS or CdSe brought a significant efficiency improvement on CdTe solar cells [7,34]. The fundamental reason is that the interdiffusion between CdS (or CdSe) and CdTe reduces the defect state density and suppresses the recombination of carriers. Selenium has less size mismatch with Te than S and therefore has a much higher solubility in CdTe. From EQE curves in Fig. 2, the high J$_{sc}$ (26.93 mA/cm^2) of the device with MZO/CdS/CdSe buffer layer indicates the strong interdiffusion at the CdS/CdSe/CdTe interface and the formation of CdSSeTe alloys, which occurred during the high temperature CdTe deposition and CdCl$_2$ heat treatment. The interdiffusion between CdS/CdSe/CdTe effectively passivates the interface of buffer/absorber and reduces the defect states, thus leading to dominant bulk recombination. Comparing with MZO and MZO/CdS cells, the MZO/CdS/CdSe cells exhibit better performance and its average efficiency has exceeded that of traditional CdS cells, showing a great promise in high efficiency CdTe solar cells.

To further illustrate the dominant recombination paths of devices, JVT measurement in dark was carried out. Fig. 5 shows the dark current-voltage characteristics of the device with MZO/CdS/CdSe buffer layer from 300 K to 355 K. The linear part of the curves shown in the dash line region represents the diode behavior of solar cells. From this region, parameters of ideality factor A and saturation dark current J_0 can be determined. The activation energy extracted by extrapolating V_{oc} to 0 K in light JVT measurement ignores the change of ideality factors with various temperature. Here, the ideality factors A of four devices are plotted versus temperature in Fig. 6. The ideality factors slightly increase with temperature for devices with CdS, MZO and MZO/CdS buffer layers but seem to temperature-independent for the device with ZMO/CdS/CdSe buffer layer. Note that there are two cases where the ideal factor exceeds 2. For the device with MZO buffer layer, the MZO film does not form a good junction with CdTe, so the p-n junction may not be ideal and the ideality factor exceeds 2. For the device with MZO/CdS/CdSe buffer layer which is dominated by bulk recombination, the ideality factor ≥ 2 is approved [35]. In addition, considering additionally tunneling enhanced recombination, diode
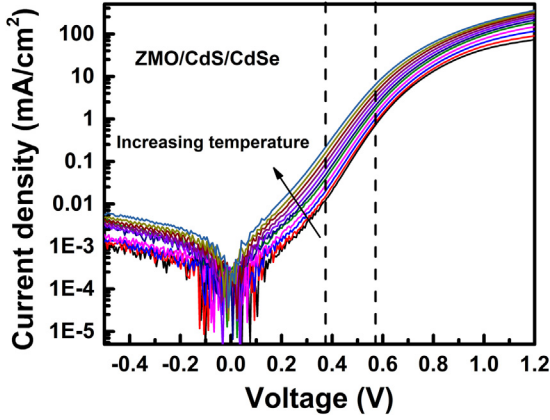
Fig. 5. The logarithmic current-voltage characteristics of CdTe solar cells with MZO/CdS/CdSe buffer layer at various temperatures in dark.
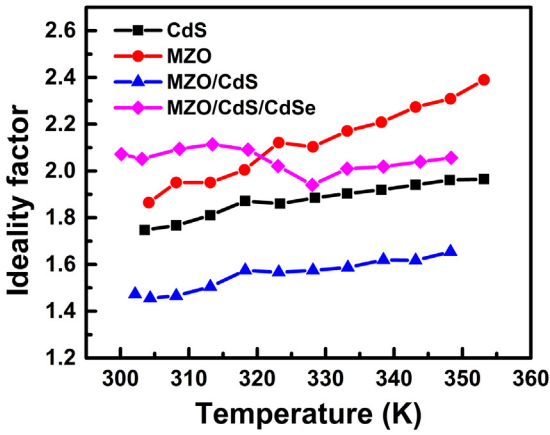

Fig. 6. The ideality factors for CdTe solar cells with different buffer layers are plotted versus temperature in dark JVT measurements.
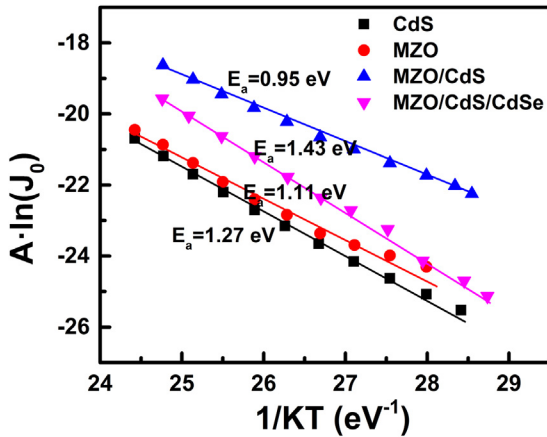

Fig. 7. The quantity $Aln(J_0)$ as a function of $1/kT$ for four devices.

Table 2
The E_a evaluated from light JVT and dark JVT measurements.

Sample	Light (A) E_a (eV)	Dark (B) E_a (eV)	Differences (A–B) E_a (eV)
CdS	1.35	1.27	0.08
MZO	1.01	1.11	− 0.10
MZO/CdS	1.06	0.95	0.11
MZO/CdS/CdSe	1.49	1.43	0.06

quality factors above 2 are possible [8,11]. The quantity $Aln(J_0)$ as a function of $1/kT$ for four devices is showed in Fig. 7. The activation energy for the saturation current deduced from the slop of $Aln(J_0)$ versus $1/kT$ is slight different from the value of extrapolated V_{oc} to 0 K. The differences are no more than ± 0.11 eV as shown in Table 2, which are mainly caused by the error of calculation. The E_a extracted from light JVT measurement introduces less errors because no parameters of one-diode model are needed. For the E_a extracted from dark JVT measurement, the parameters of A and J_0 must be calculated, thus giving a negative contribution to the value of E_a. However, the effect on the results is not very large, therefore, both two methods are reliability to illustrate the results.

The dark current-voltage curve is commonly used as an important diagnosis of recombination in solar cells. At low forward bias, recombination occurs mainly in the space charge region with an ideality factor $A ≥ 2$. At high forward bias, the composition of the quasi-neutral region increases as the minority carrier concentration rises, leading to $A = 1$ [36]. Therefore, the dominated recombination path for the CdS/CdTe device is believed to be bulk recombination. With ideality factors varying between 1.68 and 1.95, the recombination mainly occurs in the space charge region. The dominant recombination paths are interface recombination for devices with MZO or MZO/CdS buffer layers since the activation energy are much lower than bandgap energy, only 1.11 eV and 0.95 eV, respectively. The activation energy of the device with MZO/CdS/CdSe buffer layer (1.43 eV) is close to the bandgap and the diode quality equals to 2, which indicates that bulk recombination is dominant in the space charge region. The design of MZO/CdS/CdSe buffer layer suppresses the interface recombination of devices and changes the dominant recombination path of devices.

For more quantitative understanding of recombination mechanisms of carriers, TRPL was performed from which the effective decay time can be estimated. The TRPL decay curves are showed in Fig. 8. A two-exponential decay model is used to fit decay time [37]:

$$I_{PL(t)} = A_1 \exp(-t/\tau_1) + A_1 \exp(-t/\tau_2), \qquad (6)$$

where t is the time, $I_{PL(t)}$ is the time-dependent PL intensity, and A_1/A_2 are amplitude of decay components τ_1/τ_2. τ_1 is dominated by drift and diffusion, and τ_2 is probably limited by Shockley-Read-Hall recombination, which may be a better parameter for tracking bulk recombination in both the space charge region and quasi-neutral region in CdTe solar cells [38]. Therefore, τ_2 is considered as the effective decay time for comparison in this work.

One of the limitations of all analyses that employ excitation with laser pulses, such as TRPL, is absorption depth of the laser radiation. When excitation is at 630 nm, $1/\alpha_{630nm} \approx 200$ nm for CdTe (α is absorption coefficient) [39]. The decay times of the devices with CdS (60 nm) or MZO (80 nm)/CdS (30 nm)/CdSe (80 nm) buffer layers are relatively long (5.2 ns). As discussed above, the strong interdiffusion
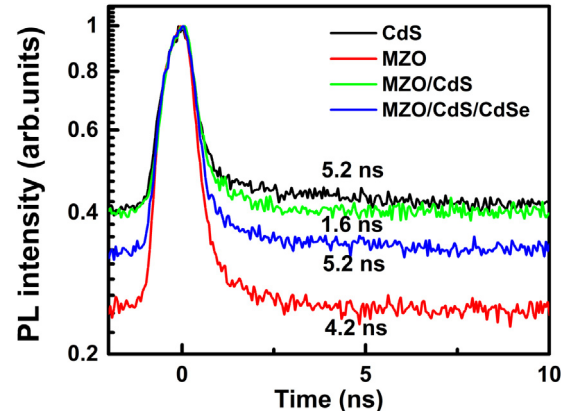

Fig. 8. TRPL decay curves for CdTe solar cells with different buffer layers.

between CdS/CdTe or CdS/CdSe/CdTe passivates the interface defects effectively and leads to dominant bulk recombination, which is consistent with the long τ_2. The decay time for the device with MZO/CdS buffer layer is only 1.6 ns because the CdS film is ultrathin (30 nm) and the interdiffusion between CdS and CdTe is not enough to passivate the interface states. The 633-nm wavelength illumination generates more carriers next to the MZO/CdTe$_{1-x}$S$_x$ interface with lots of defects thus leading to the shortest τ_2. For devices with MZO buffer layers, there is almost no interdiffusion between MZO and CdTe and its interface is abrupt, which means the interface states exist only in the very thin layer (possibly a few nanometers) at the interface. Considering the bandgap of MZO ($\sim$ 3.7 eV), the 633 nm light is transmitted through the MZO layer and into the CdTe layer ($\sim$ 200 nm). In this case, the fluorescence signals from TRPL are more influenced by CdTe absorber than the MZO/CdTe interface. Therefore, the minority carrier lifetime (4.2 ns) is long despite its interface recombination mechanism.

5. Conclusion

In this work, temperature-dependent current-voltage measurements (JVT) and time-resolved photoluminescence (TRPL) were performed to investigate the recombination mechanisms of CdTe solar cells with different buffer layers. The values of activation energy for devices with MZO and MZO/CdS buffer layers are $\sim$ 1 eV, which illustrating that the dominant recombination path is interface recombination, thus leading to low V_{oc} and poor performance of devices. The activation energy of the device with MZO/CdS/CdSe buffer layer is close to 1.5 eV, which exhibits bulk recombination to be dominant, that is, the same dominant recombination path as traditional CdS/CdTe devices. The introduction of CdSe layer modifies the buffer/absorber interface and suppresses the interface recombination. More importantly, the device with MZO/CdS/CdSe buffer layer enhances the photo current up to 26.3 mA/cm^2 and the conversion efficiency has exceeded 15%. It demonstrates that the MZO/CdS/CdSe is a successful design and can be a promising composite buffer layer in high efficiency CdTe solar cells.

Acknowledgements

References

[1] M.A. Green, Y. Hishikawa, E.D. Dunlop, D.H. Levi, J. Hohl-Ebinger, A.W.Y. Ho-Baillie, Solar cell efficiency tables (version 51), Prog. Photovolt. Res. Appl. 26 (2018) 3–12.

[2] T. Minemoto, Y. Hashimoto, W. Shams-Kolahi, T. Satoh, T. Negami, H. Takakura, Y. Hamakawa, Control of conduction band offset in wide-gap Cu(In,Ga)Se$_2$ solar cells, Sol. Energy Mater. Sol. Cells 75 (2003) 121–126.

[3] A.H. Munshi, J.M. Kephart, A. Abbas, T.M. Shimpi, K. Barth, J.M. Walls, W.S. Sampath, Effect of varying deposition and substrate temperature on sublimated CdTe thin-film photovoltaics, in: Proceedings of the Photovoltaic Specialists Conference (PVSC), 2016 IEEE 43rd, IEEE, 2016, pp. 0465–0469.

[4] A.E. Delahoy, S. Peng, P. Patra, S. Manda, A. Saraf, Y. Chen, X. Tan, K.K. Chin, Cadmium tin oxide and zinc magnesium oxide prepared by hollow cathode sputtering for CdTe photovoltaics, MRS Adv. 2.53 (2017) 3203–3214.

[5] J.M. Kephart, J.W. McCamy, Z. Ma, A. Ganjoo, F.M. Alamgir, W.S. Sampath, Band alignment of front contact layers for high-efficiency CdTe solar cells, Sol. Energy Mater. Sol. Cells 157 (2016) 266–275.

[6] T. Wang, S. Ren, C. Li, W. Li, C. Liu, J. Zhang, L. Wu, B. Li, G. Zeng, Exploring window buffer layer technology to enhance CdTe solar cell performance, Sol. Energy 164 (2018) 180–186.

[7] N.R. Paudel, Y. Yan, Enhancing the photo-currents of CdTe thin-film solar cells in both short and long wavelength regions, Appl. Phys. Lett. 105 (2014) 183510.

[8] U. Malm, J. Malmström, C. Platzer-Björkman, L. Stolt, Determination of dominant recombination paths in Cu(In,Ga)Se$_2$ thin-film solar cells with ALD–ZnO buffer layers, Thin Solid Films 480 (2005) 208–212.

[9] T. Kobayashi, Z.J.L. Kao, T. Nakada, Temperature dependent current–voltage and admittance spectroscopy on heat-light soaking effects of Cu(In,Ga)Se$_2$ solar cells

[10] with ALD-Zn(O,S) and CBD-ZnS(O,OH) buffer layers, Sol. Energy Mater. Sol. Cells 143 (2015) 159–167.

[11] T.P. Weiss, Electrical Characterization of Kesterite Thin Film Absorbers and Solar Cells, University of Luxembourg, Luxembourg, Luxembourg, 2015.

[11] J.D. Major, T.M. Al, L. Bowen, M. Brossard, C. Li, P. Lagoudakis, S.J. Pennycook, L.J. Phillips, R.E. Treharne, K. Durose, In-depth analysis of chloride treatments for thin-film CdTe solar cells, Nat. Commun. 7 (2016) 13231.

[12] R.E. Brandt, Accelerating the Development of Novel Photovoltaic Materials, Massachusetts Institute of Technology, 2016.

[13] R.E. Brandt, N.M. Mangan, J.V. Li, R.C. Kurchin, T. Milakovich, S. Levcenco, E.A. Fitzgerald, T. Unold, T. Buonassisi, Temperature- and intensity-dependent photovoltaic measurements to identify dominant recombination pathways, in: Proceedings of the Photovoltaic Specialists Conference, 2016, pp. 1997–2001.

[14] S.S. Hegedus, W.N. Shafarman, Thin-film solar cells: device measurements and analysis, Prog. Photovolt. Res. Appl. 12 (2004) 155–176.

[15] M. Bär, L. Weinhardt, C. Heske, Advanced Characterization Techniques for Thin Film Solar Cells, Wiley-VCH, 2011.

[16] J. Pettersson, C. Platzer-Björkman, M. Edoff, Temperature-dependent current-voltage and lightsoaking measurements on Cu(In, Ga)Se2 solar cells with ALD-Zn1-xMgxO buffer layers, Prog. Photovolt. Res. Appl. 17 (2009) 460–469.

[17] J. Lee, Comparison of CdS films deposited by different techniques: effects on CdTe solar cell, Appl. Surf. Sci. 252 (2005) 1398–1403.

[18] I. Dharmadasa, Review of the CdCl$_2$ treatment used in CdS/CdTe thin film solar cell development and new evidence towards improved understanding, Coatings 4 (2014) 282–307.

[19] S.S. Hegedus, B.E. McCandless, CdTe contacts for CdTe/CdS solar cells: effect of Cu thickness, surface preparation and recontacting on device performance and stability, Sol. Energy Mater. Sol. Cells 88 (2005) 75–95.

[20] A. Halverson, A. Yakimov, A. Vert, O. Sulima, B. Korevaar, Side-by-side characterization of non-optimized and optimized CdS/CdTe solar cells on commercial transparent conductive oxide/glass, Thin Solid Films 535 (2013) 249–252.

[21] J.M. Kephart, Optimization of the front contact to minimize short-circuit current losses in CdTe thin-film solar cells, Dissertations & Theses - Gradworks, 2015.

[22] G. Fonthal, L. Tirado-Mejıa, J. Marın-Hurtado, H. Ariza-Calderon, J. Mendoza-Alvarez, Temperature dependence of the band gap energy of crystalline CdTe, J. Phys. Chem. Solids 61 (2000) 579–583.

[23] J. Sites, J. Pan, Strategies to increase CdTe solar-cell voltage, Thin Solid Films 515 (2007) 6099–6102.

[24] T. Song, A. Kanevce, J.R. Sites, Emitter/absorber interface of CdTe solar cells, J. Appl. Phys. 119 (2016) 233104.

[25] A. Klein, Energy band alignment in chalcogenide thin film solar cells from photoelectron spectroscopy, J. Phys.: Condens. Matter 27 (2015) 134201.

[26] A.E. Delahoy, Z. Cheng, K.K. Chin, Evidence for CdTe$_{1-x}$S$_x$ compound formation in CdTe solar cells from high-precision, temperature-dependent device measurements, in: Proceedings of the Photovoltaic Specialists Conference, 2014, pp. 1945–1948.

[27] J.N. Duenow, R.G. Dhere, H.R. Moutinho, B. To, J.W. Pankow, D. Kuciauskas, T.A. Gessert, CdS x Te 1-x alloying in CdS/CdTe solar cells, MRS Online Proceedings Library Archive 1324, 2011.

[28] H.B. Cuong, N.M. Le, S.-H. Jeong, B.-T. Lee, Tailoring of composition, band-gap, and structural phase in ZnMgO films by simply controlling growth temperature and oxygen partial pressure during sputter deposition, J. Alloy. Compd. 709 (2017) 54–63.

[29] S. Ren, H. Wang, Y. Li, H. Li, R. He, L. Wu, W. Li, J. Zhang, W. Wang, L. Feng, Rapid thermal annealing on ZnMgO window layer for improved performance of CdTe solar cells, Sol. Energy Mater. Sol. Cells 187 (2018) 97–103.

[30] B.E. McCandless, K.D. Dobson, Processing options for CdTe thin film solar cells, Sol. Energy 77 (2004) 839–856.

[31] J. Han, C. Spanheimer, G. Haindl, G. Fu, V. Krishnakumar, J. Schaffner, C. Fan, K. Zhao, A. Klein, W. Jaegermann, Optimized chemical bath deposited CdS layers for the improvement of CdTe solar cells, Sol. Energy Mater. Sol. Cells 95 (2011) 816–820.

[32] G.V. Rao, F. Säuberlich, A. Klein, Influence of Mg content on the band alignment at CdS/(Zn,Mg)O interfaces, Appl. Phys. Lett. 87 (2005) 032101.

[33] F. Bittau, Analysis and Optimisation of Window Layers for Thin Film CDTE Solar Cells, Loughborough University, 2017.

[34] J. Britt, C. Ferekides, Thin-film CdS/CdTe solar cell with 15.8% efficiency, Appl. Phys. Lett. 62 (1993) 2851–2852.

[35] H. Wilhelm, H.-W. Schock, R. Scheer, Interface recombination in heterojunction solar cells: influence of buffer layer thickness, J. Appl. Phys. 109 (2011) 084514.

[36] S. Grover, J.V. Li, D.L. Young, P. Stradins, H.M. Branz, Reformulation of solar cell physics to facilitate experimental separation of recombination pathways, Appl. Phys. Lett. 103 (2013) 093502.

[37] D. Kuciauskas, P. Dippo, Z. Zhao, L. Cheng, A. Kanevce, W.K. Metzger, M. Gloeckler, Recombination analysis in cadmium telluride photovoltaic solar cells with photoluminescence spectroscopy, IEEE J. Photovolt. 6 (2016) 313–318.

[38] D. Kuciauskas, A. Kanevce, J.N. Duenow, P. Dippo, M. Young, J.V. Li, D.H. Levi, T.A. Gessert, Spectrally and time resolved photoluminescence analysis of the CdS/CdTe interface in thin-film photovoltaic solar cells, Appl. Phys. Lett. 102 (2013) 173902.

[39] D. Kuciauskas, A. Kanevce, J.M. Burst, J.N. Duenow, R. Dhere, D.S. Albin, D.H. Levi, R.K. Ahrenkiel, Minority carrier lifetime analysis in the bulk of thin-film absorbers using subbandgap (two-photon) excitation, IEEE J. Photovolt. 3 (2013) 1319–1324.